International Journal of Applied Electromagnetics and Mechanics 00 (0) 1–7
IOS Press

Mimicking Soft Magnetic Composite Geometries Algorithmically

Joonas Vesa [a,*], Taru Karhula [b], Antero Marjamäki [a], Jay Panchal [a] and Paavo Rasilo [a]
[a] *Laboratory of Electrical Energy Engineering, Tampere University of Technology, Korkeakoulunkatu 10, Tampere, 33720. Finland*
[b] *Laboratory of Materials Science, Tampere University of Technology, Korkeakoulunkatu 10, Tampere, 33720. Finland*

Abstract. In this paper we describe an algorithmic method to imitate geometries of soft magnetic composites. We use microscope images to determine some of the most important geometric characteristics of the material and optimize the algorithm such that the measured and simulated characteristics are in agreement. We compute the static magnetization curves using the geometries obtained from the images and the algorithm comparing the results. The aim is to produce realistic geometries to be used in homogenization schemes as well as to study the effects of magnetic contacts in general.

Keywords: geometry generation, homogenization, magnetic composite

1. Introduction

Soft magnetic composite (SMC) materials consist of small ferromagnetic particles coated with some electrical insulation material, compacted and heat treated. Some materials are sintered. These kind of materials have some significant advantages, *e.g.* isotropic behaviour in macroscopic scale and low eddy current losses since the conductivity between individual particles is relatively low [1]. These qualities make the materials appealing for applications such as high frequency inductors and transformers as well as rotating machines. Compared to the macroscopic dimensions, the particles are very small, usually some tens of micrometers. A microscope image of an SMC material is found in Figure 1a.

The multiscale nature of SMC materials makes them somewhat tedious to model since some electromagnetic phenomena, like eddy currents, are strongly affected by the particle-size geometry. There are approaches for examining the particle-size structures. Cyr *et al.* proposed a two-dimensional approach based on meshing a real microscope image [2]. The method has been adopted recently again in [3]. Cyr's approach allows capturing a lot of information about the materials but an excessive amount of imaging is required. Belkadi *et al.* proposed an algorithmic method in [4] and [5]. The algorithm was based on filling a regularly meshed reference cube which is somewhat restrictive for the geometries.

Our study aims to combine the advantages of these approaches. We intend to generate SMC geometries by postulating an algorithm and to fit its parameters such that the generated geometries mimic some of the geometric characteristics obtained from the microscope images. We compute the static magnetization curves using the geometries obtained from the microscope images and the algorithm comparing the results. It should be noted that multiscale methods and algorithmic geometry generation have been studied quite extensively in the field of applied mechanics [6] but the electromagnetic properties of such materials have so far recieved less attention.

---

[*] Corresponding author: Joonas Vesa, Laboratory of Electrical Engineering, Tampere University of Technology, Korkeakoulunkatu 10, Tampere, 33720, Finland, E-mail: joonas.vesa@tut.fi

2. Methods

In this section we describe two methods to produce geometries for the comparison in Section 4. We use a FeNiMo alloy toroid with saturation flux density of 0.9 T and relative permeability of 240 in the linear magnetization range as an example. It should be noted that this study does not aim to model a specific material. Instead we make a comparison between two methods.

2.1. *Image based approach*

The material sample was cut, molded into a support, grinded and polished [2]. Microscope images were taken using an optical microscope. In Figure 1a we see a microscope image of the material.

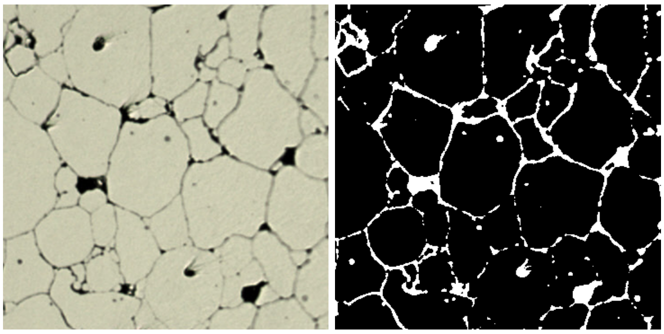

(a) A microscope image (b) A two-color version

Fig. 1. SMC geometries, FeNiMo alloy, width 280 µm

We assume that the sample consists of two distinct materials. Using an edge detection algorithm we turn the microscope image into a two-color picture (Figure 1b). We chose to take a threshold of the color intensities and we suspect that the same method is used in [3]. Every pixel is then subdivided into two triangles for finite element computations.

From Figure 1b we compute the volume fraction $\eta \approx 0.899$. Highlighting magnetic contacts between individual particles by hand with a distinctive color and computing the overall length of the colored lines, we find the relative contact length of $l_\mathrm{c} \approx 1.95$ with respect to the width of the image. We also computed the relative mean area of the particles $A_\mathrm{m} \approx 0.019$ with respect to the area of Figure 1b. We expect the method to lose a lot of information about the gaps and hence η and l_c should be considered as quite artificial. We reason this by stating that the choice of the color threshold strongly dictates these values.

2.2. *Algorithm based approach*

Instead of filling a pre-defined mesh like in [4,5], we describe the geometry independent of a mesh which may be optimized afterwards for computational purposes. Nevertheless we intend to keep the consideration simple. The ideas presented here are strongly inspired by Voronoi tessellations, which may be interpreted as a result of a ball-growth process from predefined nucleation points [7]. These methods are widely acknowledged and utilized very recently for instance in the study of polycrystalline and nanocrystalline structures [8]. In our setting the algorithm should be flexible enough to leave some room for optimization of the geometric characteristics and hence we decided not to use bare Voronoi diagrams. An example of a more flexible tessellation method is the Johnson-Mehl process [9,10] and we more or less follow these ideas.

Next we describe the algorithm briefly in suitable steps that may be implemented as collections of routines. While reading the descriptions, it is worth to keep in mind the big picture. At first we execute *initiation* and *refinement*. Here randomly placed nucleation points are added, triangles defined around them and the triangle/polygon boundaries refined by adding additional boundary points. Then the *growth* and *refinement* processess are repeated until the overall area of the particles does not significantly change. This way the polygons grow to fill more area but they do not overlap other polygons. Then *contacts are imposed* by inserting randomly placed hexagons on the boundaries of the polygons. Finally *cropping and scaling* is carried out. Finished geometry is then meshed for computational purposes. In the following some parameters of the algorithm are left undefined. We will discuss them later.

Initiation. We choose a bounding square $[0, 1] \times [0, 1]$. In Figure 2a the bounding box is represented by the dashed square. Then points $\{c_1, c_2, ..., c_N\}$ are injected randomly into the box such that the condition $d(c_j, c_i) > d_\text{p}$ is met for every $i \neq j$, where $d(\cdot, \cdot)$ is the euclidean distance and d_p is some predefined constant. We also require that no point is closer than d_p to the bounding box. Next equilateral triangles are defined around the points. For instance around the point c_1 we set the points b_1, b_2, b_3 such that $d(c_1, b_i) = d_\text{p}/3$ for $i = 1, 2, 3$ and denote the triangle (polygon) as $p_1 = (b_1, b_2, b_3)$ with a nucleation point c_1. The triangles do not overlap each other and are fully contained inside the bounding box.

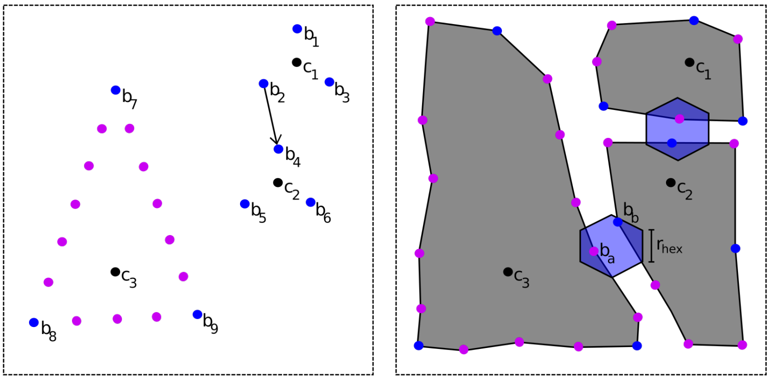

(a) Imitating the particles (b) Imitating contacts

Fig. 2. Algorithmic geometry generation

Growth. Consider the polygon p_1 (with a nucleation point c_1) and its boundary point b_2 . The point b_2 is moved to the location $b_2 + \left(d_{b_2,\text{min}} - d_\text{gap}\right)(b_2 - c_1)/d(b_2, c_1)$, where d_gap is some predefined positive constant and $d_{b_2,\text{min}}$ is computed as follows. First we compute the distance $d_{b_2,\text{point}} = \min_{b_i \notin p_1} d(b_2, b_i)$. In Figure 2a this minimum distance is denoted by an arrow between points b_2 and b_4. We also compute the minimum distance between b_2 and the bounding box. We denote this distance as $d_{b_2,\text{box}}$. We set $d_{b_2,\text{min}} = \min\{d_{b_2,\text{point}}, d_{b_2,\text{box}}\}$. This process is repeated for every boundary point of each polygon.

Refinement. Consider the polygon p_3, which has been enlarged such that the blue points b_7, b_8 and b_9 have been moved. Now we add the purple points. We loop through the points b_7, b_8 and b_9 and compute the distance between neighbouring points. Consider the point b_7. We compute the distance $d(b_7, b_8)$. Let $k = \text{floor}\,\{d(b_7, b_8)/d_\text{reso}\}$, where d_reso is some predefined positive constant. We add k new equally spaced points in the straight line between b_7 and b_8. We repeat the process for each polygon. This assures that no neighboring points in a polygon are further away from each other than d_{reso}.

Imposing contacts. Choosing some number N_{hex} of hexagons, we randomly choose N_{hex} polygon boundary points b_i with a condition $d(b_i, b_j) > d_{\text{hex}}$ using some suitable positive d_{hex}. Consider b_a in Figure 2b as one of the randomly chosen points. We consider the point $b_a + (d_{b_a,\text{min}}/2)\,(b_a - c_3)/d(b_a, c_3)$, as the 'centerpoint' of the blue hexagon with line lengths (or 'radius') of r_{hex}. Here we assume that the polygon boundaries are refined enough such that $d_{b_a,\text{min}}$ more or less corresponds to the gap width. The hexagons are added into the collection of polygons.

Cropping and scaling. We define another square $S = [l/2, 1-l/2] \times [l/2, 1-l/2]$, whose edge length is $1-l$, if $0 \le l < 1$. The geometry is defined as the set union of the polygons and hexagons intersected with S. The geometry is then scaled approproppriately.

Next we choose suitable parameters for the algorithm. Our first naive approach is to generate geometries with constant gap sizes, imposing desired contact lengths and volume fraction.

We set $N = 200$ as the initial number of particles. We set $d_{\text{p}} = 0.034$ for the minimum distance between the particle nucleation points. This affects the variation of the particle sizes. We decided to crop the generated geometries such that the final geometry has approximately the same particle mean area $A_{\text{m}} \approx 0.019$ as the microscope image if the geometries are scaled to equal sizes. This was achieved by defining the cropping square to have an edge length of 0.427, whereas the original bounding square edge length was 1.0.

We optimized the particle gap size related distance d_{gap} with linear regression. We generated sample geometries, computed their volume fractions and optimized d_{gap} to give the desired mean volume fraction $\eta \approx 0.899$ obtained from the microscope image. To ensure adequate smoothness of the particle boundaries we set $d_{\text{reso}} = d_{\text{gap}}$.

For the contacts we set the number of contacts $N_{\text{hex}} = 220$ and $d_{\text{hex}} = 0.046$, which is the minimum distance between two distinct hexagons to assure the contacts are distributed all over the domain. We optimized the contact lengths by linear regression. We generated sample geometries, computed the contact lengths with different hexagon radii r_{hex} and found that $r_{\text{hex}} = 0.0229$ gives $l_{\text{c}} \approx 1.95$ as the mean contact length. In Figure 4a we can see an algorithmically generated geometry with constant gap width.

3. Computational methods

Let us first discuss a magnetostatic nonlinear two-dimensional finite element formulation. We write $\mathbf{B} = \frac{\partial A}{\partial y}\mathbf{i} - \frac{\partial A}{\partial x}\mathbf{j}$, where A is a (z-component of a vector-) potential. Requiring Ampere's law and expressing the potential as a linear combination of finite element basis functions $\{\varphi_i\}_{i=1}^{N}$, we find the discretized residual vector

$$r_k(\bar{\alpha}) = \int_\Omega \left\langle \mathbf{H}\left(\sum_{i=1}^{N} \alpha_i \left(\frac{\partial \varphi_i}{\partial y}\mathbf{i} - \frac{\partial \varphi_i}{\partial x}\mathbf{j}\right)\right), \frac{\partial \varphi_k}{\partial y}\mathbf{i} - \frac{\partial \varphi_k}{\partial x}\mathbf{j} \right\rangle dS,$$

where $\bar{\alpha}$ is a tuple of the nodal values and $\mathbf{H}$ is a constitutive relation $\mathbf{H} = \mathbf{H}(\mathbf{B})$. Since we intend to utilize a nonlinear constitutive relation, we chose to use the Newton-Raphson scheme to solve $\bar{r}(\bar{\alpha}) = 0$.

Let us now consider the constitutive relation. In anhysteretic and isotropic setting we assume that $\mathbf{H}(\mathbf{B}) = H_{\text{sc}}(\|\mathbf{B}\|)\frac{\mathbf{B}}{\|\mathbf{B}\|}$ for an approppriate scalar function H_{sc}, which we define by $H_{\text{sc}} = B_{\text{sc}}^{-1}$. For simplicity we use the modified Langevin function for magnetization and hence

$$B_{\mathrm{sc}}(\|\mathbf{H}\|) = \mu_0\|\mathbf{H}\| + \mu_0 M_{\mathrm{sat}}\left(\coth\frac{\|\mathbf{H}\|}{a} - \frac{a}{\|\mathbf{H}\|}\right),$$

where M_{sat} characterizes the saturation magnetization and a the shape of the magnetization curve [11]. The inverse is computed numerically. In Figure 3a we see black particles and white gaps. This is again the microscope image turned into a two-color image. We use the relation $\mathbf{H} = \mathbf{H}(\mathbf{B})$ for the elements in the black regions and just inverse vacuum permeability for the whites.

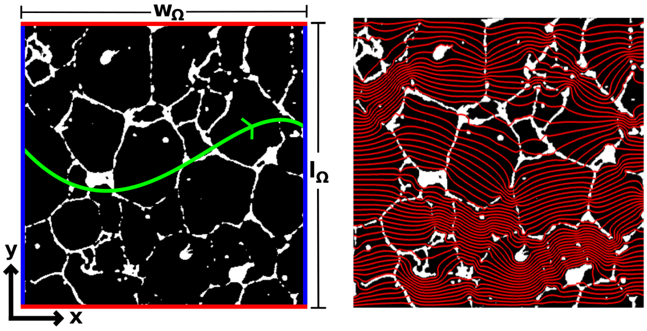

(a) Description of the domain (b) Solution for $B_{\mathrm{avg}} = 0.4$ T

Fig. 3. Setting the computational problem

Let us now consider boundary conditions. In Figure 3a we see a description of the domain Ω and its boundary. We do not set A at the blue boundary sections but the homogeneous Neumann condition is statisfied. For the bottom red boundary we set a Dirichlet condition $A = 0$. We also set for the upper red boundary $A = B_{\mathrm{avg}} l_\Omega$, where B_{avg} stands for average magnetic flux density and l_Ω the height of the domain. These conditions impose an average flux density of B_{avg} in the x-direction through the modeling domain.

Let us briefly discuss a simplistic homogenization method. We defined B_{avg} and related it to the finite element problem. We denote $H_{\mathrm{avg}} = \frac{1}{w_\Omega}\int_C \mathbf{H}\cdot\mathbf{dl}$, where w_Ω is the width of Ω and C is a curve from the left blue boundary to the right in Figure 3a. Due to Ampere's law, the absence of currents through the domain and the boundary conditions, the integral is not dependent on the curve C. By Fubini's theorem $H_{\mathrm{avg}} = \frac{1}{l_\Omega w_\Omega}\int_\Omega H_{\mathrm{x}} dS$. We use the latter one for averaging purposes since the Ampere's law is only statisfied in a weak sense. Our interest is now to compare the magnetization curves $(B_{\mathrm{avg}}, H_{\mathrm{avg}})$ obtained from the problems set by the image based approach and our algorithm based one.

4. Optimization of the algorithm and comparisons

We first estimated the constitutive model parameters $\mu_0 M_{\mathrm{sat}} \approx 1$ T and $a \approx 39$ A/m using the image based method. We set these parameters such that the linear relative permeability of $(B_{\mathrm{avg}}, H_{\mathrm{avg}})_{\mathrm{image}}$ was approximately 240 and the effective saturation was 0.9 T. These figures correspond to our example material.

We generated two hundred samples with the algorithm. Since the geometric characteristics like volume fraction are set in a statistical sense, we set an additional restriction and allowed only 0.22% error in the volume fraction neglecting others. In Figure 4a we see an example of algorithmically generated geometry. It has some overall similarities with Figure 1b. For comparison we computed the magnetization curves

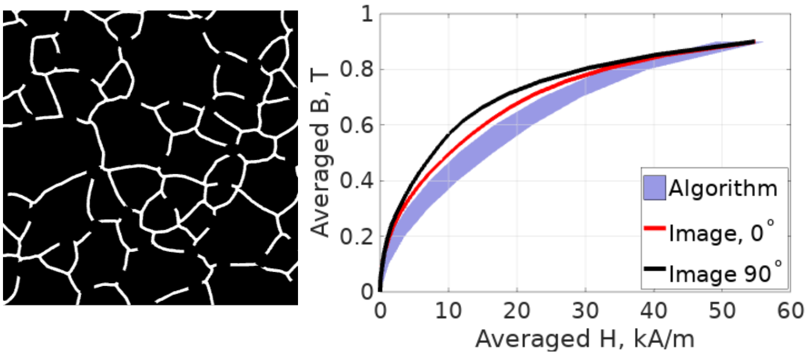

(a) Generated geometry (b) Magnetization curves

Fig. 4. Comparison of magnetization curves, algorithm with constant gap widths

twice: first using the image of Figure 1b and then with the same image rotated 90 degrees. In Figure 4b we see a comparison between the magnetization curves obtained using the image based geometries and algorithm based geometries. The algorithm related blue area represents 99% confidence limits.

We see that there is an agreement between the curves in the linear region around the origin and at saturation level but not in between. The agreement in the saturation region is due to the fixing of the volume fraction, since in saturated material in our setting the flux lines are parallel to the x-axis independently of the geometry and the volume fraction becomes a dominant factor in the magnetization. Even though there is an agreement in the linear region, as soon as the contacts saturate, the magnetization is weaker than in the image based case.

Our next attempt is to add some variation to the gap widths to achieve higher overall magnetization below the saturated regions. This may be done by correcting a couple of parameters in the algorithm. Our idea is to set a relatively high d_{gap} and before imposing contacts, we grow the particles once more by a magnitude proportional to d_{gap}. We first set the magnitude of the final enlargement as $0.48 d_{\text{gap}}$. This is a heuristically chosen value. Then we found $d_{\text{gap}} = 0.021$ by generating samples, computing volume fractions and setting d_{gap} such that $\eta \approx 0.899$ is met in statistical sense. To ensure some additional smoothness to the particles, we also set $d_{\text{reso}} = 0.2 d_{\text{gap}}$. In Figure 5a we can see an image of such geometry. The appearance of this geometry is significantly different from Figure 4a.

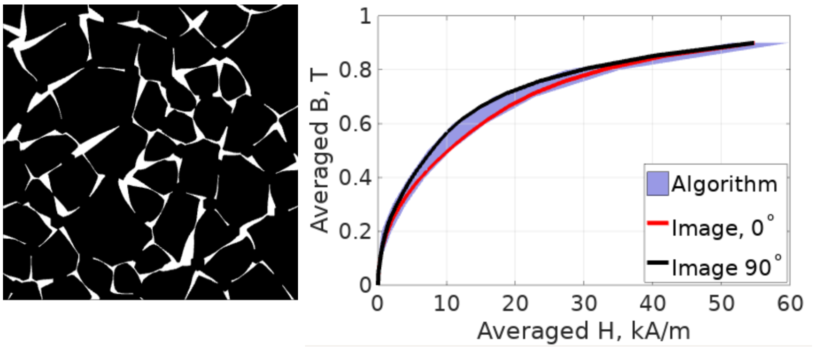

(a) Generated geometry (b) Magnetization curves

Fig. 5. Comparison of magnetization curves, algorithm with variable gap widths

We generated two hundred samples tolerating maximum 0.22% error in the volume fraction. In Figure 5b the blue area represents 99% confidence of the averaged magnetization obtained by using the algorithmically generated geometries. The agreement between the algorithm based and image based magnetization curves is significantly better than in the case of constant gap widths. We note that the additional contacts between particles were added similarly in both cases.

5. Concluding remarks

We described a method to imitate powder-like soft magnetic composite geometries algorithmically. We used two-dimensional geometries obtained from microscope images as a reference. From the images we measured some geometric characteristics like the volume fraction, magnetic contact lengths and the mean of particle areas. We then tuned our algorithm such that these parameters were in agreement. As a comparison we meshed the microscope images and generated geometries into finite element geometries and computed static magnetization curves using a very simplistic computational homogenization.

We found that fixing just the mean of particle sizes, the volume fraction and magnetic contact lengths between the material particles was not enough to capture the shape of the magnetization curves. As soon as the contacts saturated, the magnetization was weaker than in the image based simulations. The magnetization properties of powder-like composites are heavily dependent not only on contacts and the volume fraction of the material but also on the overall variations of the gaps. We also argued that the image based method is vulnerable to losing gap size information.

Our algorithm turned out to be flexible enough to allow variations in the gaps and we were able to accurately reproduce the shape of the magnetization curve obtained by the image based method. We consider the results as promising and continue to work on repeating the computations in three dimensions. Our future work focuses also on experimental validation of the local and global magnetization curves.

Acknowledgements

The foundation of Emil Aaltonen and the Academy of Finland are acknowledged for financial support.

References

[1] H. Shokrollahi, K. Janghorban, Soft magnetic composite materials (SMCs), *Journal of Materials Processing Technology*, **189(1-3)**, (2007).
[2] C. Cyr, P. Viarouge, S. Clenet and J. Cros, Methodology to Study the Influence of the Microscopic Structure of Soft Magnetic Composites on Their Global Magnetization Curve, *IEEE Transactions on Magnetics*, **45(3)**, (2009).
[3] Y. Ito, H. Igarashi, M. Suzuki, Y. Iwasaki and K. Kawano, Effect of Magnetic Contact on Macroscopic Permeability of Soft Magnetic Composite, *IEEE Transactions on Magnetics*, **52(3)**, (2016).
[4] M. Belkadi, B. Ramdane, D. Trichet and J. Fouladgar, Non Linear Homogenization for Calculation of Electromagnetic Properties of Soft Magnetic Composite Materials, *IEEE Transactions on Magnetics*, **45(10)**, (2009).
[5] M. Belkadi, D. Trichet, B. Ramdane and J. Fouladgar, Modeling of Soft Magnetic Composite Material Using a Non Linear Homogenization Method, *Proc. CEFC*, Chigago, IL, USA, May 2010. (2010).
[6] Multiscale modelling and design for engineering application, *VTT Technology 77*, Kopijyvä Oy, Kuopio 2013.
[7] S. N. Chiu, D. Stoyan, W. S. Kendall, J. Mecke, *Stochastic Geometry and its Applications*, John Wiley & Sons, Ltd., 2013.
[8] S. Falcoa, J. Jiang, F. De Cola, N. Petrinica, Generation of 3D polycrystalline microstructures with a conditioned Laguerre-Voronoi tessellation technique, *Computational Materials Science*, **136**, (2017).
[9] W. A. Johnson, R. F. Mehl, Reaction kinetics in processes of nucleation and growth, *Transactions of the American Institute of Mining, Metallurgical and Petroleum Engineers*, **135**, (1939).
[10] A. Okabe, B. Boots, K. Sugihara, S. N. Chiu, *Spatial Tessellations*, John Wiley & Sons, Ltd., 2000.
[11] D. C. Jiles, D. L. Atherton, Theory of Ferromagnetic Hysteresis, *Journal of Magnetism and Magnetic Materials*, **61**, (1986).